


Photocatalytic Activity of Boron Doped CuO and Its Composite with Polyaniline

Hafize Nagehan Koysuren & Ozcan Koysuren

To cite this article: Hafize Nagehan Koysuren & Ozcan Koysuren (2023) Photocatalytic Activity of Boron Doped CuO and Its Composite with Polyaniline, Polymer-Plastics Technology and Materials, 62:3, 281-293, DOI: [10.1080/25740881.2022.2113894](https://doi.org/10.1080/25740881.2022.2113894)

To link to this article: <https://doi.org/10.1080/25740881.2022.2113894>

 View supplementary material [↗](#)

 Published online: 21 Aug 2022.

 Submit your article to this journal [↗](#)

 Article views: 77

 View related articles [↗](#)

 View Crossmark data [↗](#)

RESEARCH ARTICLE



Photocatalytic Activity of Boron Doped CuO and Its Composite with Polyaniline

Hafize Nagehan Koysuren^a and Ozcan Koysuren^b

^aDepartment of Environmental Engineering, Kirsehir Ahi Evran University, Kirsehir, Turkey; ^bDepartment of Energy Engineering, Ankara University, Ankara, Turkey

ABSTRACT

This study used a simple one-step technique to prepare boron-doped copper (II) oxide (CuO-B) nanoparticles, which were synthesized through the solution combustion method. The as-prepared CuO-B nanoparticles were compounded with the conducting polymer, polyaniline (Pani), in varying composition. This study revealed the effect of compounding with Pani on the photocatalytic activity of CuO-B. The photocatalytic activity was evaluated through the degradation of the methylene blue dye under visible light irradiation. The as-prepared CuO-B nanoparticles and their composites with Pani were characterized through Fourier-transform infrared spectroscopy, X-ray powder diffraction spectroscopy, fluorescence spectroscopy, scanning electron microscopy and UV–Vis absorption spectroscopy. When compared with CuO-B, Pani composites resulted in improved photocatalytic dye degradation efficiency due to the suppression of the recombination rate of the photoexcited charge carriers on CuO-B. The Pani composite with 80 wt.% CuO-B exhibited an 65.3% degradation of the model dye in 240 min, which was about 7% higher than that of CuO-B. A 1.2-fold increase in the reaction rate was obtained for the specified composite. The optical band gap of CuO-B increased to 1.40 eV when it was compounded with 20 wt.% Pani. In real wastewater environment, the dye degradation efficiency of CuO-B decreased from 57.9% to 51.9%. In addition, the dye degradation efficiency of four times of recycled CuO-B reduced to 33.7% in 240 min.

ARTICLE HISTORY

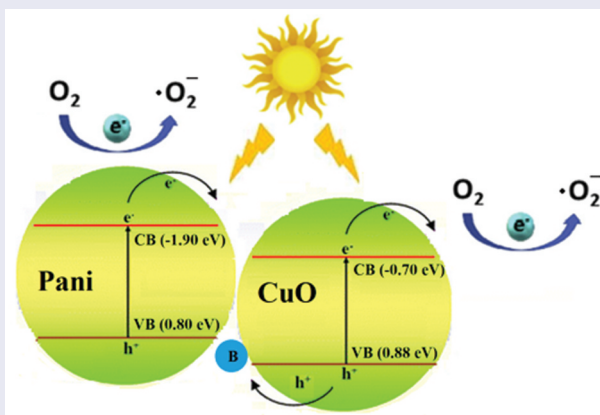
Received 31 May 2022

Revised 21 July 2022

Accepted 12 August 2022

KEYWORDS

Photocatalytic activity; photocatalytic dye degradation; copper (II) oxide; polyaniline; polymer composite




1. Introduction

Water pollution is one of the most challenging issues across the world. Although different types of pollutants are produced, dyes are still the principal pollutants that cause harmful effects on human beings and environment due to their non-biodegradable and toxic properties.^[1] Especially, azo dyes are widely utilized in various processes owing to their high activity. There are also simple azo dyes like anionic and cationic dyes, which include hydroxyl groups in their chemical

structure and do not form a strong chemical bond with the dyed material. Azo dyes are composed of both natural and synthetic organic compounds and are known as stable organic pollutants.^[2] There is a growing interest in the treatment of the wastewater including organic dyes since the organic dye molecules are considered to be a potential risk to the human health and the environmental sustainability.^[3] The organic dye molecules are extensively discharged into the environment, leading to serious water and soil pollution owing to biological

CONTACT Ozcan Koysuren  koysuren@ankara.edu.tr 

 Supplemental data for this article can be accessed online at <https://doi.org/10.1080/25740881.2022.2113894>

© 2022 Taylor & Francis

degradation, high chemical oxygen demand (COD) of water, and toxicity on humans.^[4] The organic dye molecules can enter the body of living things through ingestion, and they can be metabolized by intestinal microorganisms, giving rise to DNA damage.^[5] They can also cause hormonal and endocrine disruptions in living organisms.^[6] The organic dyes have a wide range of applications in the cosmetic, textile, and pharmaceutical industries. The wastewater effluent of the textile plants has been considered to be the most polluting among all the industries. Among the various organic dyes, methylene blue, known as a toxic cationic dye, is difficult to degrade naturally due to its stability to various oxidation reactions. For this reason, it has often been used as a model dye for organic pollutants in many studies. Thus, the removal of organic dye molecules from the wastewater becomes important in terms of environmental and human health.^[4] Several techniques have been applied to remove organic dye molecules from wastewater such as sedimentation, flotation, adsorption, ion exchange, coagulation-flocculation, sonocatalytic degradation, precipitation, microbial degradation, electrochemical treatment, Fenton process, and photocatalytic degradation.^[1,3,6] Among the noticed techniques, the photocatalytic dye degradation has attracted more attention because of the advantages of high removal rate, environmental friendliness, and cost-effectiveness.^[3,5] The photocatalytic dye degradation is a process in which the photogenerated electron-hole pairs are formed on a photocatalyst upon exposure to UV light or visible light irradiations. The photoexcited charge carriers can react with surface adsorbed water and oxygen molecules to form hydroxyl and superoxide radicals, which can convert the organic dye molecules into small harmless molecules.^[7]

CuO has been considered to be one of the promising photocatalysts owing to its low cost and toxicity. In addition, CuO has been regarded as one of the narrow band-gap semiconductors suitable for visible light application. The main drawbacks of CuO as a photocatalyst are the fast recombination of the photogenerated charge carriers and poor stability in harsh environmental conditions.^[3] To solve the recognized problems, various strategies like metal or nonmetal doping, coupling CuO with another semiconductor or a conducting polymer have been followed.^[3] Metal or nonmetal doping can lead to the formation of structural defects in the crystal structure of CuO, which can act as a trapping center for the photoexcited charge carriers. Thus, metal or nonmetal doping can suppress the recombination of the photogenerated electron-hole pairs.^[8] Until now, many dopant atoms including platinum,^[8] cerium,^[9] lanthanum,^[10] silver,^[11] nitrogen atom,^[12] and carbon atom^[13] enhanced the

Table 1. Literature data on photocatalytic dye degradation efficiency in the presence of photocatalysts combined with CuO.

Photocatalyst	Model dye	Irradiation time	Photocatalytic degradation efficiency
ZnO ^[1]	Methylene blue	60 min	99.2%
Cu ₂ O ^[11]	Methyl orange & methylene blue	60 min	84.2%
CoTiO ₃ ^[12]	Methylene blue	120 min	85.0%
TiO ₂ ^[13]	Rhodamine B	60 min	40.0%
WO ₃ ^[14]	Acid red 88	180 min	62.0%
Polyaniline ^[15]	Chlorpyrifos	90 min	95.0%
Polythiophene ^[16]	Methylene blue	90 min	83.2%

photocatalytic performance in disparate applications. Among the noticed strategies, several studies have been performed to enhance the photocatalytic activity of CuO by coupling with semiconductors such as ZnO,^[1] Cu₂O,^[14] CoTiO₃,^[15] TiO₂,^[16] and WO₃,^[17] respectively (Table 1). In addition, several studies have been reported in which polyaniline,^[18] polythiophene,^[19] and polypyrrole,^[20] separately, were compounded with CuO to enhance its photocatalytic performance (Table 1). Conducting polymers, possessing π -bonds on their backbone, are known as an attractive alternative to the semiconductor photocatalysts. Due to the presence of free electrons along their chains, they can provide improved photocatalytic performance and more active sites for photocatalytic reactions.^[18] In the presence of a light source, electrons from CuO and another semiconductor or conducting polymer are induced to the conduction band, forming the photoexcited holes in the valence band. Based on the band potential differences, the photogenerated electron-hole pairs can be separated, suppressing the recombination of the photoinduced charge carriers.^[1]

In this study, boron-doped CuO nanoparticles were synthesized, and they were compounded with polyaniline to reduce the rapid recombination rate of the photogenerated charge carriers formed on CuO under visible light irradiation. To the best of our knowledge, no studies have been reported in the literature on the photocatalytic activity of the boron-doped CuO and its composite with polyaniline. The boron atom has rarely been used as a dopant in photocatalytic activity studies. At the same time, CuO is not much preferred as a photocatalyst. In this respect, doping CuO with boron and using it in the photocatalytic dye degradation studies are important.

2. Experimental

2.1. Synthesis of Boron-Doped CuO and Preparation of Polyaniline Composites

The solution combustion technique was followed to synthesize the boron-doped CuO nanoparticles. To

prepare the boron doped CuO, copper nitrate ($\text{CuO}(\text{NO}_3)_2 \cdot 3\text{H}_2\text{O}$) and citric acid ($\text{C}_6\text{H}_8\text{O}_7 \cdot \text{H}_2\text{O}$) were used as the precursor chemicals. The copper nitrate to citric acid ratio was kept as unity. Stoichiometric amount of copper nitrate (1.0 g) and citric acid (0.869 g) was dissolved in 30 ml of distilled water. Boric acid (H_3BO_3) as boron (B) atom source was added into the copper nitrate-citric acid solution. The weight ratios of B to CuO were adjusted to be 1%, 3%, and 5%, respectively. Then, the solution was kept under stirring on a plate at 100°C . Initially, the solution started to boil and it underwent the dehydration reaction. Afterward, the solution in the gel form started to decompose with the release of all volatile components, converting the gel into black powders. The as-prepared powder was ground and calcinated at 400°C for 4 hours.^[21] The CuO nanoparticles doped with 1, 3, and 5 wt.% B atoms were named as CuO-B1, CuO-B3, and CuO-B5, respectively.

Polyaniline composites differing in the content of CuO-B were synthesized using the in-situ polymerization technique. For this purpose, aniline hydrochloride (0.518 g) was dissolved in 50 ml of distilled water to prepare a 4 mM monomer solution. Various amounts of the boron-doped CuO were suspended in the as-prepared monomer solution. CuO-B1, providing the highest photocatalytic dye degradation efficiency, was utilized to prepare the composites. The CuO-B1 content of the composites was adjusted to be 20, 40, 60, and 80 wt.%, respectively. On the other hand, ammonium peroxydisulfate (1.141 g) was dissolved in 50 ml of distilled water to prepare a 5 mM oxidant solution. Then, the oxidant solution was added into the monomer solution. The final suspension was kept under stirring at room temperature. The polymerization of aniline hydrochloride was expected to be completed within 24 hours. The composite particles were collected on a filter and rinsed with acetone to prevent agglomeration. Finally, the composite nanoparticles were dried at 60°C .^[22] The composite samples were labeled as CuO-B1/Pani(x/100-x) (x = 20, 40, 60, 80), respectively.

2.2. Methods of Characterization

Fourier-transform infrared (FTIR) spectroscopy of the samples was recorded at a resolution of 4 cm^{-1} in the range of 400 cm^{-1} to 4000 cm^{-1} using Perkin Elmer 400 model spectrophotometer. X-ray diffraction pattern of the samples was obtained in the range of 20° to 70° using Inel Equinox 1000 model X-ray diffractometer operated with a $\text{CoK}\alpha$ radiation source. X-ray photoelectron spectroscopy (XPS) of the samples was recorded by using PHI 5000 VersaProbe model XPS instrument operating

with a monochromated Al $\text{K}\alpha$ radiation source (1486.6 eV). Fluorescence emission spectrum of the samples was measured with Lumina model fluorescence spectrophotometer (Thermo Scientific) at the excitation wavelength of 320 nm. The morphology of the samples was accessed by QUANTA 400 F model field emission scanning electron microscope (FESEM). UV-Vis absorption spectrum of the samples was measured using a UV-Vis spectrophotometer (Genesys 10S, Thermo Scientific) in the range of 200 to 800 nm.

The photocatalytic dye degradation efficiency of the samples was studied using methylene blue as a model dye in an aqueous solution under visible light irradiation. Methylene blue (1 mg) was dissolved in 100 ml of distilled water, and the photocatalyst sample (50 mg) was dispersed in the dye solution. The suspension was kept under stirring in the absence of irradiation for half an hour to ensure equilibrium of the as-prepared suspension. Then, the suspension was exposed to visible light irradiation by using a 300 W lamp (Osram Ultravitalux). A distance of about 15 cm was set between the visible light lamp and the suspension. The photocatalytic activity test unit was ventilated using a fan to keep the temperature of the suspension constant. The photocatalytic dye degradation was monitored using the UV-Vis spectrophotometer. Test samples were collected at regular time intervals (30 min). The photocatalyst nanoparticles were removed from the solution by centrifuging. The supernatant solution was utilized by the UV-Vis spectroscopy to determine the photocatalytic dye degradation rate using the following equation (1).^[23] In addition, the following pseudo-zero-order (2)^[24] and pseudo-first-order (3)^[25] kinetic models were used to study the reaction kinetics of the methylene blue degradation.

$$\text{Dye degradation rate\%} = (C_0 - C)/C_0 \quad (1)$$

$$C_0 - C = kt \quad (2)$$

$$\ln(C_0/C) = kt \quad (3)$$

where C_0 was the initial concentration of methylene blue and C was the concentration of the model dye after the visible light irradiation. The reaction rate constant (k) was determined from the slope of the $(C_0 - C)$ vs. time (t) and $\ln(C_0/C)$ vs. t graphs of the samples, respectively.

To understand the details of the photocatalytic degradation mechanism, scavenger tests were performed with CuO-B1. For this purpose, tert-butanol (6 ml/100 ml dye solution), a hydroxyl radical scavenger,^[26] and ascorbic acid (1 mg/100 ml dye solution), a superoxide radical

scavenger,^[27] were added into the methylene blue solution prior to the photocatalytic degradation test. To study the effect of the ambient condition on the photocatalytic activity, pH of the methylene blue solution was changed to 4 and 10 by using HCl (0.1 M) and NaOH (0.1 M), respectively. In addition, the effect of the real wastewater condition on the photocatalytic activity was studied. The real wastewater sample, supplied by Ankara central wastewater treatment plant, was used to prepare the methylene blue solution, and CuO-B1 was added into the as-prepared dye solution. After 30 min stirring under the dark ambient, the suspension was exposed to the visible light irradiation. To study the stability of the prepared photocatalysts, the reusability test was applied to the CuO-B1 sample. After the photocatalytic degradation test, CuO-B1 was separated from the dye solution by centrifuging and rinsed with distilled water. Following the drying, it was added into a newly prepared methylene blue solution for the next degradation cycle. Four successive degradation cycles were studied using the same procedure.

3. Results and Discussion

3.1. FTIR Analysis

FTIR spectrum of CuO-B1 exhibits two main transmittance peaks at around 480 cm^{-1} and 590 cm^{-1} , which were attributed to the stretching vibration of Cu-O bond.^[28] In addition, FTIR spectrum of CuO-B1 exhibits a broad transmittance band at round 1365 cm^{-1} , which was related to symmetrical stretching vibration of the B-O bond (Figure 1a).^[29] FTIR spectrum of CuO-B1 confirmed the successful synthesis of CuO and doping of the boron atom into the CuO chemical structure.^[28,29] FTIR spectrum of the CuO-B1/Pani(80/20) composite illustrates characteristic transmittance peaks at around 778 cm^{-1} , 1085 cm^{-1} , 1230 cm^{-1} , 1494 cm^{-1} , and

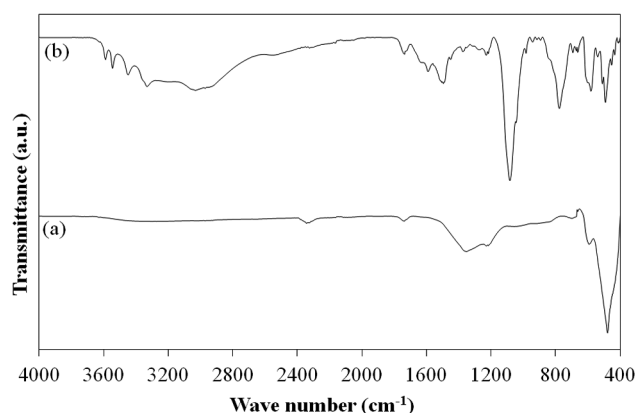


Figure 1. FTIR spectra of (a) CuO-B1 and (b) CuO-B1/Pani(80/20).

1589 cm^{-1} (Figure 1b), which were attributed to the out-of-plane C-H stretching, the 1, 4-substitution on the benzene ring, the C-N stretching vibration, the C = C stretching vibration of benzene ring and the C = C stretching vibration of quinone ring, respectively.^[30] The peak at 778 cm^{-1} might result from the C-H stretching vibration of benzene ring on polyaniline. The presence of this peak might be a sign for the formation of long polyaniline chains.^[31] Long polyaniline chains might contribute to the photocatalytic activity of the composite due to the enhanced electrical conductivity. FTIR spectrum of the composite sample exhibits the characteristic transmittance peaks of CuO-B1 at around 493 cm^{-1} and 583 cm^{-1} . There are small changes in the wave number of the transmission peaks belonging to CuO-B1, which might be due to the interaction between the composite constituents. FTIR spectrum of the composite sample confirmed the successful synthesis of Pani in the presence of CuO-B1.

3.2. XRD Analysis

Figure 2 presents XRD spectrum of CuO-B1 and CuO-B1/Pani(80/20). All the diffraction peaks observed at $2\theta = 37.4^\circ$, 40.7° , 44.3° , 50.8° , 56.6° , 61.9° , 67.6° , 71.6° , and 75.2° were indexed to (-111) , (200) , (-112) , (-202) , (202) , (-113) , (-311) , (220) , and (312) planes of the monoclinic CuO crystal (JCPDS No. 05-0661) (Figure 2a). XRD spectrum of CuO-B1 exhibits sharp and intense diffraction peaks, indicating the synthesis of well-defined or crystallized CuO-B nanoparticles.^[9] There are two additional diffraction peaks on the XRD spectrum of CuO-B1 at around 41.7° and 48.6° , which might be due to a new phase in the crystal structure of CuO-B1. The average crystal size calculated using the Scherrer formula was 7.89 nm with CuO-B1.^[32] Figure 2b illustrates a broad band at around 25° , which was related to the amorphous Pani phase of the

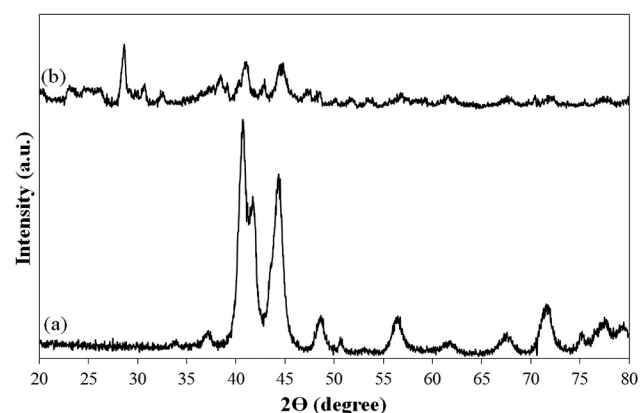


Figure 2. XRD spectra of (a) CuO-B1 and (b) CuO-B1/Pani(80/20).

composite.^[33] For the CuO-B1/Pani(80/20) composite, the characteristic diffraction peaks of CuO-B1 were observed at 38.4°, 41.0°, 44.8°, 50.2°, 56.9°, 61.7°, 67.8°, 72.3°, and 77.5°, respectively. Compared with CuO-B1, the addition of Pani broadened the diffraction peaks and greatly reduced the peak intensity, suggesting that Pani might disturb the crystal structure of CuO-B1 to a certain extent.^[34] On the other hand, the average crystal size of CuO-B1 in Pani calculated using the Scherrer formula was 13.72 nm.^[32] According to the Scherrer formula, there was an increase in the average crystal size of CuO-B1 within the polymer matrix.

3.3. XPS Analysis

The overall spectrum of CuO-B1 and CuO-B3 is presented in Figure 3a, confirming the presence of the boron atom with Cu and O atoms. In addition to the peaks belonging to Cu, O, and B atoms, there is a peak attributed to the C atom on the overall spectrum of the boron-doped CuO. The reason for the peak belonging to the C atom might arise from the chemicals used to synthesize CuO-B. Figure 3b exhibits Cu 2p spectrum of CuO-B1 and CuO-B3, respectively. Two peaks present at around 931.9 eV and 951.9 eV were assigned to Cu 2p_{3/2} and Cu 2p_{1/2} of Cu²⁺ in the CuO lattice. The energy difference between the Cu 2p_{1/2} level and the Cu 2p_{3/2} level is 20.0 eV, which is consistent with the split

orbit of Cu²⁺ ion. In addition, there are two satellite peaks at around 941.7 eV and 961.4 eV, which also indicated the Cu²⁺ state of copper atom in the CuO lattice.^[31] O 1s spectrum of CuO-B1 and CuO-B3 exhibits two peaks at around 528.6 eV and 530.2 eV, which were assigned to the O²⁻ state of oxygen atom in the CuO lattice (Figure 3c).^[35] The Cu 2p spectrum and the O 1s spectrum confirmed the successful synthesis of the CuO chemical structure. Only one peak was observed at around 191 eV on the XPS spectrum of both CuO-B1 and CuO-B3, which was attributed to the substituted boron atom with a neighbor atom vacancy (Figure 3d).^[36] The noticed peak revealed the presence of the boron atom within the CuO structure.

3.4. Fluorescence Analysis

The fluorescence spectrum of CuO-B1 and CuO-B1/Pani(80/20) illustrates two emission bands at around 506 nm and 666 nm, respectively (Figure 4). The fluorescence band observed at around 506 nm might be due to the oxygen vacancy, which can emit an emission peak as a result of the recombination of a photoinduced hole with a singly ionized electron in the valence band of CuO-B. Another fluorescence band observed at around 666 nm might be due to the surface defects, which can generate a new energy state between the conduction band and the valence band of CuO-B1 (Figure 4). This

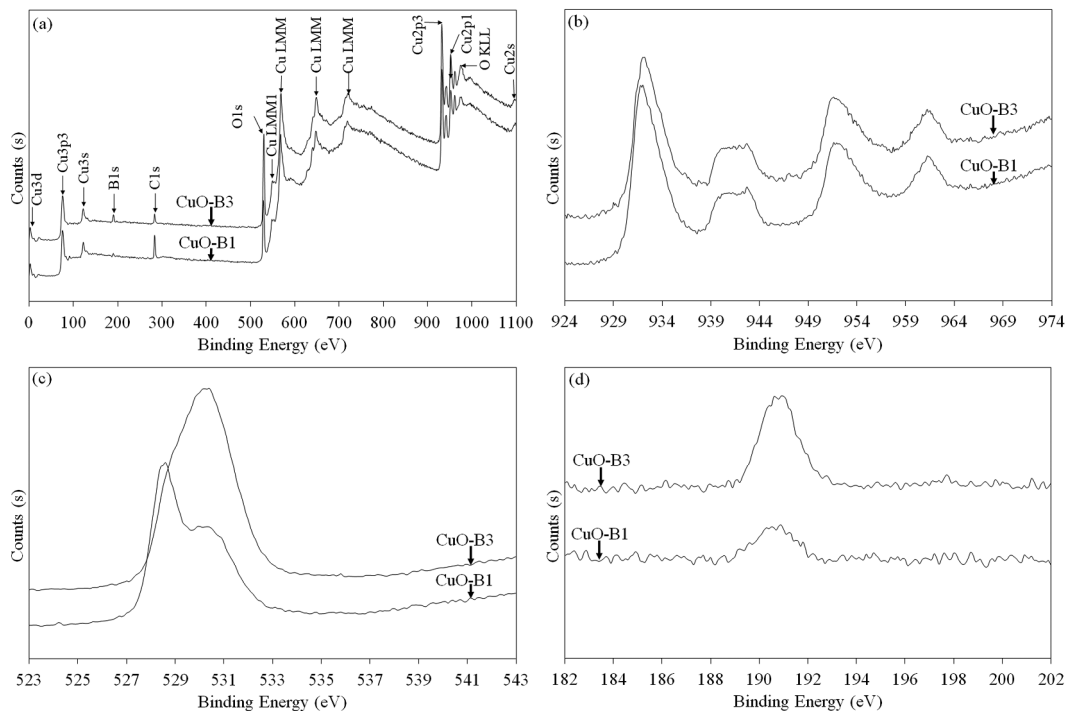


Figure 3. (a) XPS general survey spectrum and high resolution XPS spectrum of (b) Cu 2p, (c) O 1s, and (d) B 1s obtained for the boron-doped CuO.

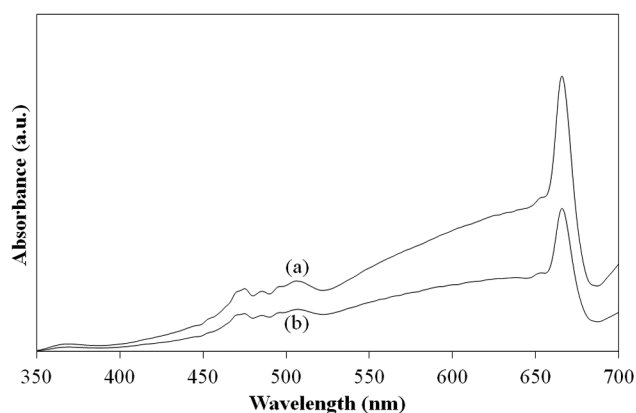


Figure 4. Fluorescence spectrum of (a) CuO-B1 and (b) CuO-B1/Pani(80/20).

energy state might behave as a trapping state to capture the photoinduced hole of CuO, helping to reduce the recombination rate of the photoinduced electron-hole pairs on CuO-B1.^[37] In addition, the intensity of the emission bands on the spectrum of CuO-B1/Pani(80/20) was lower than that of CuO-B1 (Figure 4a and 4b), which implied that combining CuO-B1 with Pani reduced the recombination rate of the photoinduced electron-hole pairs on CuO-B1.

3.5. Morphological Analysis

Figure 5 exhibits FESEM images of CuO-B1, CuO-B3, CuO-B1/Pani(40/60) and CuO-B1/Pani(80/20), respectively. According to Figure 5a and 5b, FESEM images of CuO-B1 and CuO-B3 exhibit sphere-like structures and irregular structures together. The average size of the

CuO-B1 and CuO-B3 nanoparticles varied between 200 and 400 nm. It was clearly observed that the increase in boron atom content did not affect the morphology of CuO nanoparticles. According to Figure 5c and 5d, CuO-B1 nanoparticles were uniformly dispersed in Pani matrix. In addition, they were coated with a thin polymer layer. FESEM images of the composite samples exhibit good interaction between the composite constituents. A dense composite structure was obtained by the noticed composites. Although the CuO-B1/Pani(40/60) and CuO-B1/Pani(80/20) samples contain different amounts of Pani, there is not much difference in the thickness of the Pani layer covering the CuO-B1 nanoparticles.

3.6. UV-Vis Absorption Spectroscopy

The optical properties of CuO-B and its composites are illustrated in Figure 6a and 6b, respectively. The absorption spectrum of the boron-doped CuO exhibits two bands between 200 and 250 nm and 250 and 700 nm, respectively. The broad band observed between 250 and 700 nm was attributed to the surface plasmon absorption of the boron-doped CuO. The collective oscillation of the excited free electron on the conduction band of the boron-doped CuO might be the reason for the noticed absorption band.^[38] The maximum light absorption ability seemed to be obtained by CuO-B1. The absorption spectrum of the composites illustrates two bands at around 350 nm and 750 nm, which were assigned to the π - π^* transition of the benzenoid structure belonging to Pani and to the localized polaron formation on the backbone of Pani, respectively.^[39] As

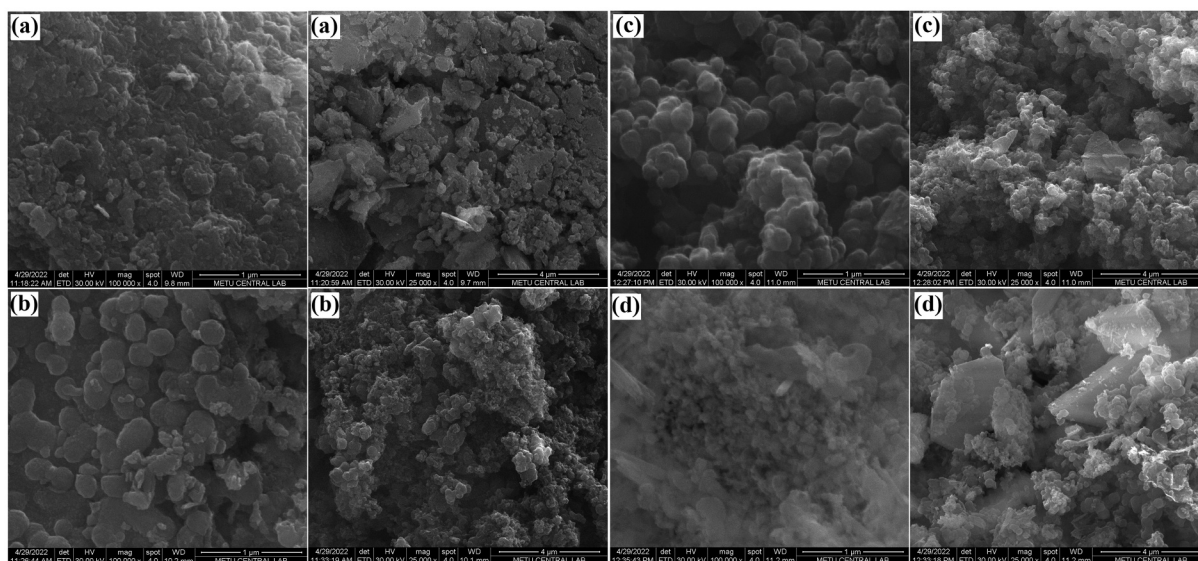


Figure 5. FESEM images of (a) CuO-B1, (b) CuO-B3, (c) CuO-B1/Pani(40/60) and (d) CuO-B1/Pani(80/20).

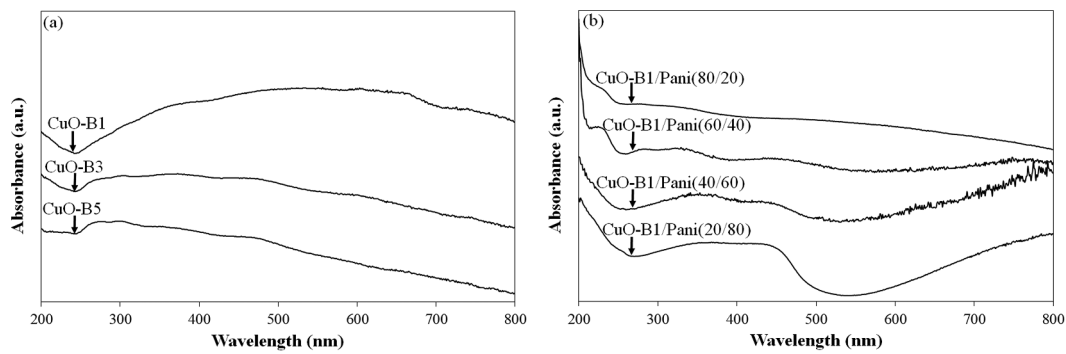


Figure 6. UV-Vis absorbance spectra of (a) CuO-B and (b) CuO-B1/Pani.

the CuO-B1 content of the composite decreased, the intensity of the absorption bands increased. The photocatalytic dye degradation tests were performed using a visible light source, providing radiation between 300 and 1000 nm. Based on the UV-Vis absorption spectroscopy results, both the boron-doped CuO and its composite with Pani can absorb the incoming light of the visible light source.

The optical band gap energy of the samples was estimated by the fitment of the absorbance data to the Tauc equation given below (4).^[38]

$$(\alpha h\nu)^2 = A(h\nu - E_g) \quad (4)$$

at which A, $h\nu$, and E_g indicate the energy-independent coefficient, the photon energy, and the

optical band gap energy, respectively. The band gap fitment spectrum of the samples is given in Figures 7 and 8. The estimated band gap values for CuO-B1, CuO-B3, and CuO-B5 were 1.25 eV, 1.55 eV, and 1.70 eV, respectively (Figure 7). The optical band gap of CuO-B widened by increasing the boron atom content, which might be linked to the Burstein-Moss effect. An increase in the boron content might increase the charge carrier concentration of the boron-doped CuO. Additional charge carriers might fill the lowest energy states of the conduction band, which could lift the Fermi energy level into the conduction band of the boron-doped CuO and result in the broadening of the optical band gap.^[40] The estimated band gap values for CuO-B1/Pani(80/20), CuO-B1/Pani(60/40), CuO-B1/Pani(40/60), and CuO-B1/Pani(20/80) were 1.40 eV, 1.60 eV, 1.90 eV, and

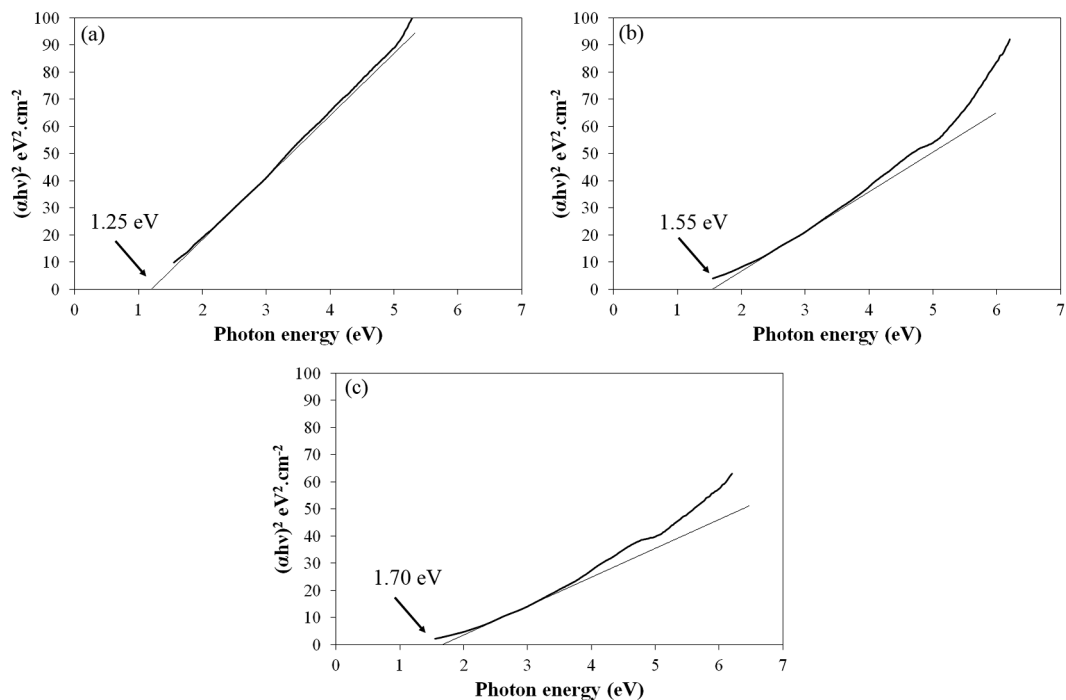


Figure 7. Tauc's plot for (a) CuO-B1, (b) CuO-B3 and (c) CuO-B5.

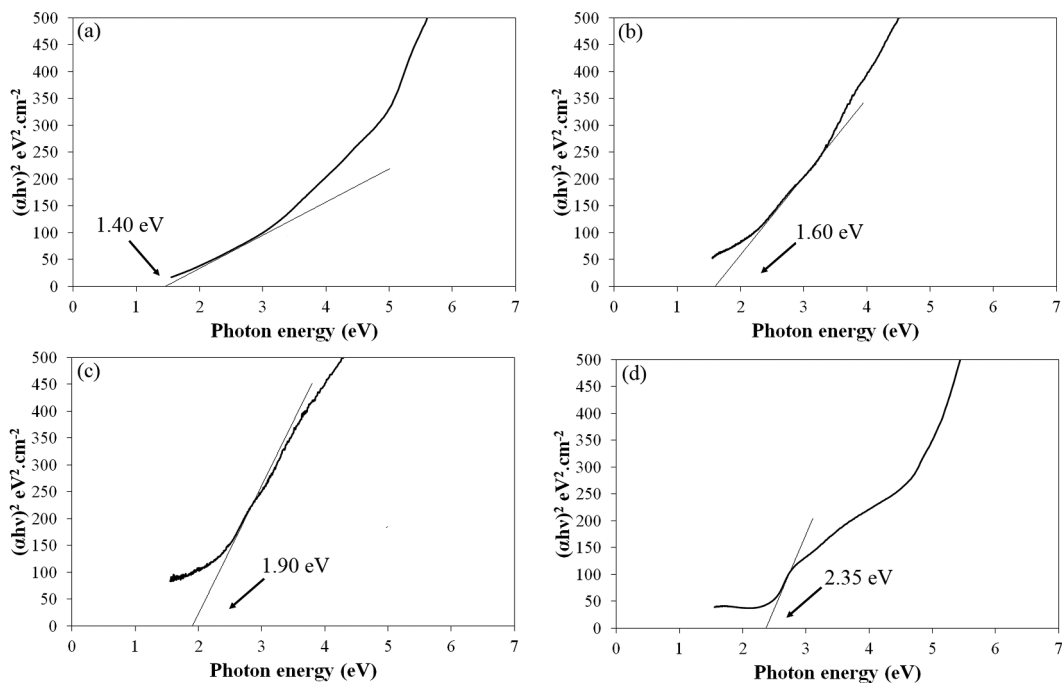


Figure 8. Tauc's plot for (a) CuO-B1/Pani(80/20), (b) CuO-B1/Pani(60/40), (c) CuO-B1/Pani(40/60) and (d) CuO-B1/Pani(20/80).

2.35 eV, respectively (Figure 8). Compared to CuO-B1, the composites had a wider band gap and the estimated band gap value continued to increase in parallel with the increase in the Pani content of the composite.

3.7. Photocatalytic activity

Figure S1 illustrates absorbance changes of the model dye, including the boron-doped CuO nanoparticles. Figure 9a exhibits the photodegradation of methylene blue in the presence of CuO-B1, CuO-B3, and CuO-B5. The photocatalytic degradation of the specified samples was 57.9%, 56.5%, and 40.7%, respectively. Based on the photocatalytic degradation results, the highest degradation efficiency was obtained by CuO-B1. Boron atom might act as a trapping center to capture the

photoexcited holes of CuO-B. Also, boron doping might increase the diffusion length of the charge carriers, prolonging the lifetime of the photoinduced electron-hole pairs. Both effects of boron doping could reduce the recombination rate of the photoexcited charge carriers.^[41] It was thought that B^{3+} ions (0.23 Å) with a smaller diameter than that of Cu^{+2} ion could diffuse into the interstitial sites of the CuO crystal.^[42] When compared with CuO-B1, lower photocatalytic efficiency was obtained with CuO-B3 and CuO-B5, respectively. Dopant atoms can induce lattice defects into the crystal structure. The specified defects can be thought as beneficial in terms of the formation of oxidation centers. However, when the dopant atom concentration in the semiconductor is too high, the dopant atoms might act as recombination centers, preventing

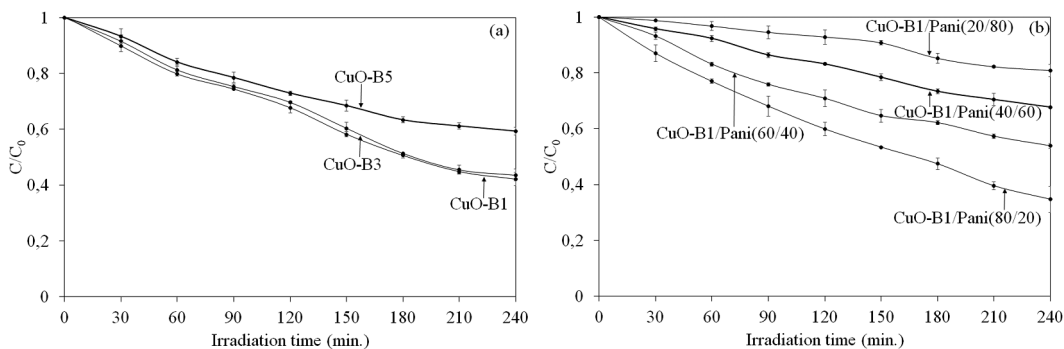


Figure 9. Photocatalytic degradation rate of methylene blue over (a) CuO-B and (b) CuO-B1/Pani under visible light irradiation.

the photoinduced charge carriers from reaching the surface of the photocatalyst.^[41]

Figure S2 exhibits absorption spectral changes of methylene blue over the CuO-B1/Pani composites. The model dye with CuO-B1/Pani(80/20) exhibited lower absorbance peaks when compared with CuO-B1 (Figure S2), indicating the success of combining the boron-doped CuO with Pani in terms of the photocatalytic activity. The photocatalytic degradation rate of methylene blue within 240 min was 65.3%, 46.2%, 32.4%, and 19.1% in the presence CuO-B1/Pani(80/20), CuO-B1/Pani(60/40), CuO-B1/Pani(40/60), and CuO-B1/Pani (20/80), respectively, under the visible light irradiation (Figure 9b). Compounding CuO-B1 with Pani might suppress the recombination rate of the photoexcited charge carriers on CuO-B1. In the composite structure, the photogenerated electrons might transport into the conduction band of CuO from the conduction band of Pani. In addition, the photogenerated holes of CuO-B1 might transport from the valence band of CuO-B1 into the valence band of Pani (Figure 10).^[43,44] Only, the CuO-B1/Pani(80/20) composite provided high photocatalytic degradation efficiency compared to CuO-B1. The synergistic composite effect could not be observed with the other compositions. As the Pani content of the composite increased, CuO-B1 nanoparticles might be covered with a thick polymer layer, preventing the contact of the photocatalyst nanoparticles with the dye molecules and the photocatalytic degradation reaction.

The reaction rate constant values, which were obtained from Figure S3 and S4, are listed in Table 2. According to the pseudo-first order kinetic model, the reaction rate constant value obtained with the CuO-B1/Pani(80/20) composite was approximately 1.2 times higher than the *k* value of CuO-B1. Among the

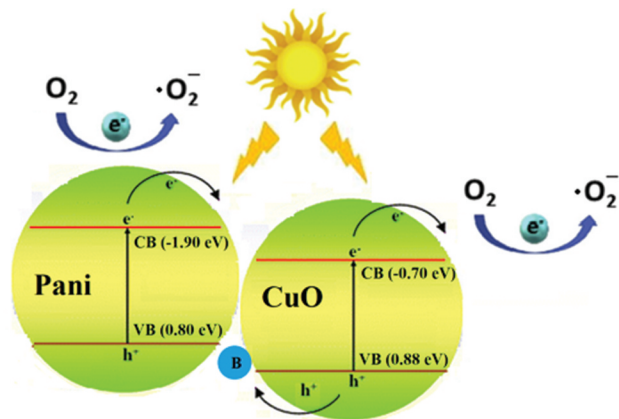


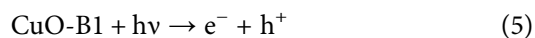
Figure 10. Proposed photocatalytic degradation mechanism of CuO-B with Pani.

Table 2. Reaction rate constant values adjusted according to the pseudo-zero-order and the pseudo-first-order kinetic models.

Sample	According to the pseudo-zero-order kinetic model		According to the pseudo-first-order kinetic model	
	<i>k</i> (min ⁻¹)	<i>R</i> ²	<i>k</i> (min ⁻¹)	<i>R</i> ²
CuO-B1	0.0264	0.9782	0.0037	0.9928
CuO-B3	0.0255	0.9851	0.0035	0.9872
CuO-B5	0.0194	0.9417	0.0024	0.9773
CuO-B1/Pani(80/20)	0.0294	0.9653	0.0043	0.9976
CuO-B1/Pani(60/40)	0.0212	0.9543	0.0027	0.9889
CuO-B1/Pani(40/60)	0.0141	0.9947	0.0016	0.9948
CuO-B1/Pani(20/80)	0.0076	0.9536	0.0008	0.9410

composite samples, an increase in the Pani content of CuO-B1/Pani reduced the reaction rate constant value. The reaction rate constant value obtained with the CuO-B1/Pani(80/20) sample was almost four times higher than the reaction rate value of the CuO-B1/Pani(20/80) composite. When both models were compared, it was thought that the photocatalytic dye degradation data were more compatible with the pseudo-first-order kinetic model since its *R*² values were closer to 1.

To study the effect of active radicals on the photocatalytic dye degradation reaction, superoxide radical ($\cdot\text{O}_2^-$) and hydroxyl radical ($\cdot\text{OH}$) scavengers were added to the reaction medium of CuO-B1. The photocatalytic dye degradation efficiency of CuO-B1 for methylene blue with the superoxide radical scavenger and the hydroxyl radical scavenger were found to be 35.0% and 56.0%, respectively (Figure 11a). There was a significant decrease and slight decrease in the photocatalytic activity of the specified photocatalyst with the superoxide scavenger and the hydroxyl scavenger, respectively. Compared to the hydroxyl radical, the superoxide radical contributed more to the photocatalytic degradation of methylene blue. When CuO-B1 absorbs the incoming light, electrons in the CuO-B1 valence band are excited to the conduction band of the photocatalyst, leading to the formation of holes in the valence band (5). The photoexcited hole can react with the hydroxide molecule in the solution to form hydroxyl radical (6). The photoexcited electrons in the conduction band can react with the dissolved oxygen molecules in the solution to generate superoxide radical. The superoxide radicals can react either with dissolved organic molecules to generate harmless degradation products (7) or with hydrogen ion (H^+) in the solution to form hydrogen peroxide radical (H_2O_2) (8) and then hydroxyl radical (9).^[45]



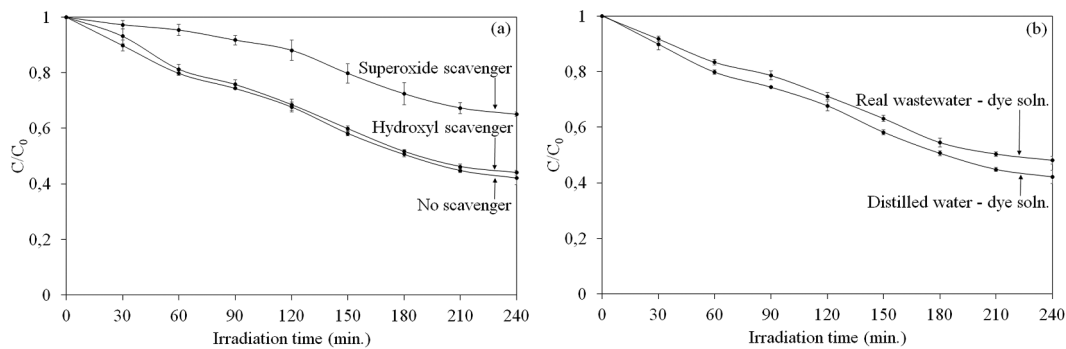
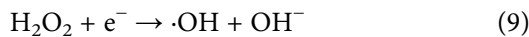
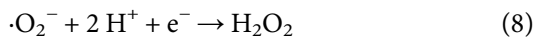


Figure 11. (a) Photocatalytic degradation rate of methylene blue with radical scavengers in the presence of CuO-B1; (b) Photocatalytic removal rate of methylene blue prepared using distilled water and real wastewater, respectively.



According to the radical scavenger test, the superoxide radical was the active radical during the photocatalytic dye degradation experiments, and the majority of the superoxide radicals generated on the photocatalyst surface might degrade organic molecules instead of forming hydrogen peroxide molecules and then hydroxyl radicals.

The photocatalytic dye degradation experiment was also performed with the dye solution prepared using the real wastewater. The degradation rate of the model dye solution prepared using distilled water and wastewater by CuO-B1 was 57.9% and 51.9%, respectively, in 240 min (Figure 11b). There was a slight decrease in the dye degradation efficiency, which was linked to the reduction in the effective surface area of the photocatalyst for the photocatalytic reaction. The active surface area of the CuO-B1 nanoparticles might reduce as

a result of the dissolved molecules in the real wastewater, which can block the active surface area of the photocatalyst nanoparticles. Possible reduction in the active surface area of the photocatalyst can reduce the photocatalytic dye degradation efficiency.

The photocatalytic degradation rate of methylene blue for four times of recycled CuO-B1 was 33.7% after 240 min of visible light irradiation (Figure 12a). According to the recycle test, CuO-B1 retain 58.0% of its photocatalytic feature at the end of four photocatalytic cycles. During the photocatalytic reaction, there might be intermediate degradation products, adsorbing on CuO-B1 and blocking the active surface area of it. The decrease in the photocatalytic activity might be attributed to the intermediate products.

The effect of pH changes on the photocatalytic activity was also studied. The photocatalytic degradation rate of methylene blue for CuO-B1 increased from 57.9% to 70.0% after 240 min of the visible light irradiation at pH = 10 (Figure 12b). On the other hand, the photocatalytic degradation rate of methylene blue for CuO-B1 decreased from 57.9% to 49.8% within 240 min at pH = 4

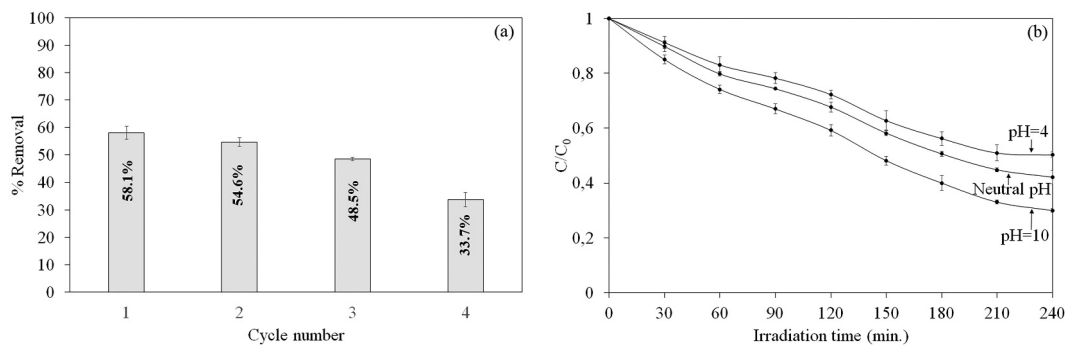


Figure 12. (a) Photocatalytic removal rate of methylene blue in the presence of recycled CuO-B1; (b) Effect of pH changes on the photocatalytic degradation rate of methylene blue in the presence of CuO-B1.

(Figure 12b). When the pH of the methylene blue solution was basic, the pH of the solution might be above CuO-B1's point of zero charge.^[44] Thus, the surface of CuO-B1 might become negatively charged, which enhanced the electrostatic attraction between the positively charged dye molecules and CuO-B1 nanoparticles.^[46] The improvement in the photocatalytic activity at high pH was attributed to the enhanced electrostatic attraction between methylene blue and CuO-B1. When the pH of the dye solution was acidic, the pH of the solution might be below CuO-B1's point of zero charge.^[44] Therefore, the surface of CuO-B1 nanoparticles might be positively charged, causing an electrostatic repulsion between the positively charged dye molecules and the photocatalyst nanoparticles.

4. Conclusions

The solution combustion technique was applied to synthesize the boron-doped CuO nanoparticles. Combining CuO-B1 with Pani in the composite structure enhanced the photocatalytic dye degradation efficiency under the visible light irradiation. The difference between the band potentials of CuO-B1 and Pani might suppress the recombination rate of the photogenerated charge carriers on CuO-B1. Based on the radical scavenger experiments, the superoxide radical was more active compared to the hydroxyl radical in the photocatalytic dye degradation reaction. CuO-B1 seemed to be highly recyclable with a slight decrease in the activity after four consecutive cycles. The real wastewater medium did not affect the photocatalytic activity of CuO-B1 much. The most important advantage of this work was to combine a rarely studied photocatalyst with a rarely used dopant atom. The biggest disadvantage was that the low photocatalytic efficiency of CuO could not be increased much. As a conclusion, the boron-doped CuO and its composite with Pani could be considered as a promising photocatalyst to degrade organic dyes within the wastewater.

Biographical note

Dr H. Nagehan Koysuren was born in Konya (Turkey) in 1982. She received her B.S. degree from Selcuk University (Konya, Turkey) in 2004 and Ph.D. degree from the same university in 2013. Dr Koysuren started her academic career as a research assistant in the Environmental Engineering department of Selcuk University in 2006, and she is working as Asst. Prof. in the Environmental Engineering department of Ahi Evran University (Kirsehir, Turkey). Dr Koysuren's research interests include photocatalytic activity, wastewater treatment, polymer composites, and heavy metal adsorption.

Dr Ozcan Koysuren was born in Dinslaken (Germany) in 1979. He received his B.S. degree from Middle East Technical

University (Ankara, Turkey) in 2002 and Ph.D. degree from the same University in 2008. Dr Koysuren started her academic career as a research assistant in the Chemical Engineering department of Middle East Technical University in 2002, and he is working as Assoc. Prof. in the Energy Engineering department of Ankara University (Ankara, Turkey). Dr Koysuren's research interests include photocatalytic activity, electrical properties, polymer composites, and polymer synthesis.

Disclosure statement

No potential conflict of interest was reported by the author(s).

Funding

This research has been supported by Ankara University Scientific Research Projects Coordination Unit. Project Number: 22H0443001, 2022.

Notes on contributor

Dr. H. Nagehan Koysuren was born in Konya (Turkey) in 1982. She received her B.S. degree from Selcuk University (Konya, Turkey) in 2004 and Ph.D. degree from the same University in 2013. Dr. Koysuren started her academic career as a research assistant in the Environmental Engineering department of Selcuk University in 2006 and she is working as Asst. Prof. in the Environmental Engineering department of Ahi Evran University (Kirsehir, Turkey). Dr. Koysuren's research interests include photocatalytic activity, wastewater treatment, polymer composites and heavy metal adsorption. *Dr. Ozcan Koysuren* was born in Dinslaken (Germany) in 1979. He received his B.S. degree from Middle East Technical University (Ankara, Turkey) in 2002 and Ph.D. degree from the same University in 2008. Dr. Koysuren started her academic career as a research assistant in the Chemical Engineering department of Middle East Technical University in 2002 and he is working as Assoc. Prof. in the Energy Engineering department of Ankara University (Ankara, Turkey). Dr. Koysuren's research interests include photocatalytic activity, electrical properties, polymer composites and polymer synthesis.

ORCID

Hafize Nagehan Koysuren  <http://orcid.org/0000-0002-7115-2250>

Ozcan Koysuren  <http://orcid.org/0000-0001-7100-0399>

References

- [1] Thatikayala, D.; Min, B. Ginkgo Leaves Extract-assisted Synthesis of ZnO/CuO Nanocrystals for Efficient UV-induced Photodegradation of Organic Dyes and Antibacterial Activity. *J. Mater. Sci. Mater. Electron.* 2021, 32, 17154–17169. DOI: 10.1007/s10854-021-06169-x.

- [2] Al-Musawi, T. J.; Mengelizadeh, N.; Al Rawi, O.; Balarak, D. Capacity and Modeling of Acid Blue 113 Dye Adsorption onto Chitosan Magnetized by Fe₂O₃ Nanoparticles. *J. Polym. Environ.* **2022**, *30*, 344–359. DOI: [10.1007/s10924-021-02200-8](https://doi.org/10.1007/s10924-021-02200-8).
- [3] Bai, W. D.; Wu, M. B.; Du, X. L.; Gong, W. L.; Ding, Y. H.; Song, C. H.; Liu, L. Synergistic Effect of multiple-phase rGO/CuO/Cu₂O Heterostructures for Boosting Photocatalytic Activity and Durability. *Appl. Surf. Sci.* **2021**, *544*, 148607. DOI: [10.1016/j.apsusc.2020.148607](https://doi.org/10.1016/j.apsusc.2020.148607).
- [4] Rahmani, S.; Zeynizadeh, B.; Karami, S. Removal of Cationic Methylene Blue Dye Using Magnetic and Anionic-cationic Modified Montmorillonite: Kinetic, Isotherm and Thermodynamic Studies. *Appl. Clay Sci.* **2020**, *184*, 105391. DOI: [10.1016/j.clay.2019.105391](https://doi.org/10.1016/j.clay.2019.105391).
- [5] Arunadevi, R.; Kavitha, B.; Rajarajan, M.; Suganthi, A.; Jeyamurugan, A. Investigation of the Drastic Improvement of Photocatalytic Degradation of Congo Red by Monoclinic Cd, Ba-CuO Nanoparticles and Its Antimicrobial Activities. *Surf. Interfaces.* **2018**, *10*, 32–44. DOI: [10.1016/j.surf.2017.11.004](https://doi.org/10.1016/j.surf.2017.11.004).
- [6] Balarak, D.; Zafariyan, M.; Igwegbe, C. A.; Onyechi, K. K.; Ighalo, J. O. Adsorption of Acid Blue 92 Dye from Aqueous Solutions by Single-Walled Carbon Nanotubes: Isothermal, Kinetic, and Thermodynamic Studies. *Environ. Process.* **2021**, *8*, 869–888. DOI: [10.1007/s40710-021-00505-3](https://doi.org/10.1007/s40710-021-00505-3).
- [7] Islam, M. R.; Saiduzzaman, M.; Nishat, S. S.; Kabir, A.; Farhad, S. F. U. Synthesis, Characterization and Visible Light-responsive Photocatalysis Properties of Ce Doped CuO Nanoparticles: A Combined Experimental and DFT Plus U Study. *Colloid Surf. A-Physicochem. Eng. Asp.* **2021**, *617*, 126386. DOI: [10.1016/j.colsurfa.2021.126386](https://doi.org/10.1016/j.colsurfa.2021.126386).
- [8] Gadah, R. H.; Basaleh, A. S. Influence of Doped Platinum Nanoparticles on Photocatalytic Performance of CuO-SiO₂ for Degradation of Acridine Orange Dye. *Ceram. Int.* **2020**, *46*(2), 1690–1696. DOI: [10.1016/j.ceramint.2019.09.141](https://doi.org/10.1016/j.ceramint.2019.09.141).
- [9] Chen, Y. J.; Tan, H. W.; Wu, X. Q.; Sun, Q. M.; Wang, D. G.; Wang, Y. Q. Effect of Doping Ce Ions on Morphology and Photocatalytic Activity of CuO Nanostructures. *Cryst. Res. Technol.* **2019**, *54*, 1900033. DOI: [10.1002/crat.201900033](https://doi.org/10.1002/crat.201900033).
- [10] Rodney, J. D.; Deepapriya, S.; Vinosha, P. A.; Krishnan, S.; Priscilla, S. J.; Daniel, R.; Das, S. J. Photo-Fenton Degradation of Nano-structured La Doped CuO Nanoparticles Synthesized by Combustion Technique. *Optik.* **2018**, *161*, 204–216. DOI: [10.1016/j.ijleo.2018.01.125](https://doi.org/10.1016/j.ijleo.2018.01.125).
- [11] Parvathiraja, C.; Shailajha, S. Bioproduction of CuO and Ag/CuO Heterogeneous Photocatalysis-photocatalytic Dye Degradation and Biological Activities. *Appl. Nanosci.* **2021**, *114*, 1411–1425. DOI: [10.1007/s13204-021-01743-5](https://doi.org/10.1007/s13204-021-01743-5).
- [12] Ardekani, S. R.; Rouhaghdam, A. S.; Nazari, M. N-doped ZnO-CuO Nanocomposite Prepared by One-step Ultrasonic Spray Pyrolysis and Its Photocatalytic Activity. *Chem. Phys. Lett.* **2018**, *705*, 19–22. DOI: [10.1016/j.cplett.2018.05.052](https://doi.org/10.1016/j.cplett.2018.05.052).
- [13] Hosseini, S. M. H.; Moakhar, R. S.; Soleimani, F.; Sadrnezhaad, S. K.; Masudy-Panah, S.; Katal, R.; Seza, A.; Ghane, N.; Ramakrishna, S. One-pot Microwave Synthesis of Hierarchical C-doped CuO Dandelions/g-C₃N₄ Nanocomposite with Enhanced Photostability for Photoelectrochemical Water Splitting. *Appl. Surf. Sci.* **2020**, *530*, 147271. DOI: [10.1016/j.apsusc.2020.147271](https://doi.org/10.1016/j.apsusc.2020.147271).
- [14] Sahu, K.; Bisht, A.; Khan, S. A.; Sulania, I.; Singhal, R.; Pandey, A.; Mohapatra, S. Thickness Dependent Optical, Structural, Morphological, Photocatalytic and Catalytic Properties of Radio Frequency Magnetron Sputtered Nanostructured Cu₂O-CuO Thin Films. *Ceram. Int.* **2020**, *46*(10), 14902–14912. DOI: [10.1016/j.ceramint.2020.03.017](https://doi.org/10.1016/j.ceramint.2020.03.017).
- [15] Yulizar, Y.; Gunluardi, J.; Apriandanu, D. O. B.; Syahfitri, T. W. W. CuO-modified CoTiO₃ via Catharanthus Roseus Extract: A Novel Nanocomposite with High Photocatalytic Activity. *Mater. Lett.* **2020**, *277*, 128349. DOI: [10.1016/j.matlet.2020.128349](https://doi.org/10.1016/j.matlet.2020.128349).
- [16] Ren, S.; Zhang, J.; Lu, H.; Gao, S.; Li, L.; Rong, P.; Zhang, X.; Liu, Y.; Sang, D. 3D Carambola-Like CuO/TiO₂ Nanotube Heterostructures via Low-Temperature Solution Process for Photocatalytic Activity. *Eur. J. Inorg. Chem.* **2021**, *2021*(19), 1852–1857. DOI: [10.1002/ejic.202100110](https://doi.org/10.1002/ejic.202100110).
- [17] Katsumata, H.; Oda, Y.; Kaneco, S.; Suzuki, T. Photocatalytic Activity of Ag/CuO/WO₃ under Visible-light Irradiation. *RSC Adv.* **2013**, *3*(15), 5028–5035. DOI: [10.1039/c3ra23322g](https://doi.org/10.1039/c3ra23322g).
- [18] Nekooie, R.; Shamspur, T.; Mostafavi, A. Novel CuO/TiO₂/PANI Nanocomposite: Preparation and Photocatalytic Investigation for Chlorpyrifos Degradation in Water under Visible Light Irradiation. *J. Photochem. Photobiol. A-Chem.* **2021**, *407*, 113038. DOI: [10.1016/j.jphotochem.2020.113038](https://doi.org/10.1016/j.jphotochem.2020.113038).
- [19] Kalyani, R.; Gurunathan, K. Intercalated Network of Graphene Oxide (GO)-CuO-polythiophene (Pth) Hybrid Nanocomposite for Photocatalytic Applications. *J. Mater. Sci.-Mater. Electron.* **2016**, *27*(10), 10634–10641. DOI: [10.1007/s10854-016-5160-7](https://doi.org/10.1007/s10854-016-5160-7).
- [20] Mahdi, R.; Alsultan, M.; Al-Keisy, A.; Swiegers, G. F. Photocatalytic Hydrogen Generation from pH-Neutral Water by a Flexible Tri-Component Composite. *Catal. Lett.* **2020**, *151*(6), 1700–1706. DOI: [10.1007/s10562-020-03427-1](https://doi.org/10.1007/s10562-020-03427-1).
- [21] Umadevi, M.; Christy, A. J. Synthesis, Characterization and Photocatalytic Activity of CuO Nanoflowers. *Spectrosc. Acta Pt. A-Molec. Biomolec. Spectr.* **2013**, *109*, 133–137. DOI: [10.1016/j.saa.2013.02.028](https://doi.org/10.1016/j.saa.2013.02.028).
- [22] Bober, P.; Stejskal, J.; Spirkova, M.; Trchova, M.; Varga, M.; Prokes, J. Conducting Polyaniline-montmorillonite Composites. *Synth. Met.* **2010**, *160*(23–24), 2596–2604. DOI: [10.1016/j.synthmet.2010.10.010](https://doi.org/10.1016/j.synthmet.2010.10.010).
- [23] Ramirez-Aparicio, J.; Samaniego-Benitez, J. E.; Murillo-Tovar, M. A.; Benitez-Benitez, J. L.; Munoz-Sandoval, E.; Garcia-Betancourt, M. L. Removal and Surface Photocatalytic Degradation of Methylene Blue on Carbon Nanostructures. *Diam. Relat. Mat.* **2021**, *119*, 108544. DOI: [10.1016/j.diamond.2021.108544](https://doi.org/10.1016/j.diamond.2021.108544).
- [24] Fatimah, I.; Prakoso, N. I.; Sahrani, I.; Musawwa, M. M.; Sim, Y. L.; Kooli, F.; Muraza, O. Physicochemical Characteristics and Photocatalytic Performance of

- TiO₂/SiO₂ Catalyst Synthesized Using Biogenic Silica from Bamboo Leaves. *Heliyon*. 2019, 5(11), e02766. DOI: 10.1016/j.heliyon.2019.e02766.
- [25] Wang, X. H.; Li, J. G.; Kamiyama, H.; Moriyoshi, Y.; Ishigaki, T. Wavelength-sensitive Photocatalytic Degradation of Methyl Orange in Aqueous Suspension over Iron(III)-doped TiO₂ Nanopowders under UV and Visible Light Irradiation. *J. Phys. Chem. B*. 2006, 110(3), 6804–6809. DOI: 10.1021/jp060082z.
- [26] Nguyen, V. H.; Bui, Q. T. P.; Vo, D. V. N.; Lim, K. T.; Bach, L. G.; Do, S. T.; Nguyen, T. V.; Doan, V. D.; Nguyen, T. D.; Nguyen, T. D. Effective Photocatalytic Activity of Sulfate-Modified BiVO₄ for the Decomposition of Methylene Blue under LED Visible Light. *Materials*. 2019, 12(17), 2681. DOI: 10.3390/ma12172681.
- [27] Omrani, N.; Nezamzadeh-Ejehieh, A. A Ternary Cu₂O/BiVO₄/WO₃ nano-composite: Scavenging Agents and the Mechanism Pathways in the Photodegradation of Sulfasalazine. *J. Mol. Liq.* 2020, 315, 113701. DOI: 10.1016/j.molliq.2020.113701.
- [28] Anu, T.; Kumar, K. N.; Sharma, K. K. Application of Co-doped Copper Oxide Nanoparticles against Different Multidrug Resistance Bacteria. *Inorg. Nano-Met. Chem.* 2020, 50(10), 933–943. DOI: 10.1080/24701556.2020.1728554.
- [29] Wan, Q.; Zhang, J. L.; Zhang, B. X.; Tan, D. X.; Yao, L.; Zheng, L. R.; Zhang, F. Y.; Liu, L. F.; Cheng, X. Y.; Han, B. X. Boron-doped CuO Nanobundles for Electroreduction of Carbon Dioxide to Ethylene. *Green Chem.* 2020, 22(9), 2750–2754. DOI: 10.1039/d0gc00730g.
- [30] Wang, M. X.; Yun, H.; Tan, K. Q.; Guo, A. Q.; Ling, J. W.; Jiang, F. F.; Shen, X. X.; Xu, Q. J. One-step Electrochemical Synthesis of Poly(vinyl Pyrrolidone) Modified Polyaniline Coating on Stainless Steel for High Corrosion Protection Performance. *Prog. Org. Coat.* 2020, 149, 105908. DOI: 10.1016/j.porgcoat.2020.105908.
- [31] Li, X. B.; Rafie, A.; Smolin, Y. Y.; Simotwo, S.; Kalra, V.; Lau, K. K. S. Engineering Conformal Nanoporous Polyaniline via Oxidative Chemical Vapor Deposition and Its Potential Application in Supercapacitors. *Chem. Eng. Sci.* 2019, 194, 156–164. DOI: 10.1016/j.ces.2018.06.053.
- [32] Chauhan, A.; Verma, R.; Batoor, K. M.; Kumari, S.; Kalia, R.; Kumar, R.; Hadi, M.; Raslan, E. H.; Imran, A. Structural and Optical Properties of Copper Oxide Nanoparticles: A Study of Variation in Structure and Antibiotic Activity. *J. Mater. Res.* 2021, 36, 1496–1509. DOI: 10.1557/s43578-021-00193-7.
- [33] Sharma, S.; Singh, K. L.; Kumar, M.; Prasher, S. Structural, Optical and Thermal Properties of PVC/Polyaniline Composite Thin Films. *JOM.* 2022, 74, 354–360. DOI: 10.1007/s11837-021-04851-3.
- [34] Kathalingam, A.; Ramesh, S.; Yadav, H. M.; Choi, J. H.; Kim, H. S.; Kim, H. S. Nanosheet-like ZnCo₂O₄@nitrogen Doped Graphene Oxide/Polyaniline Composite for Supercapacitor Application: Effect of Polyaniline Incorporation. *J. Alloy. Compd.* 2020, 830, 154734. DOI: 10.1016/j.jallcom.2020.154734.
- [35] Soleimani, E.; Moghaddami, R. Synthesis, Characterization and Thermal Properties of PMMA/CuO Polymeric Nanocomposites. *J. Mater. Sci. Mater. Electron.* 2018, 29, 4842–4854. DOI: 10.1007/s10854-017-8440-y.
- [36] Furukawa, R.; Yamamoto, Y.; Nabei, Y.; Bandow, S. Doping of Boron or Nitrogen to Multilayered Graphene Grown on Copper by Thermal Chemical Vapor Deposition of Methane and Vapor of Phenylboronic Acid or Melamine. *MRS Adv.* 2019, 4, 211–216. DOI: 10.1557/adv.2019.26.
- [37] Suganthi, N.; Thangavel, S.; Pushpanathan, K. Infra-Red Emission and Electrochemical Properties of CuO/ZnO Nanocubes. *J. Inorg. Organomet. Polym.* 2020, 30, 5224–5233. DOI: 10.1007/s10904-020-01700-9.
- [38] Navada, K. M.; Nagaraja, G. K.; D'Souza, J. N.; Kouser, S.; Ranjitha, R.; Manasa, D. J. Phyto Assisted Synthesis and Characterization of Scoparia dulcis L. Leaf Extract Mediated Porous Nano CuO Photocatalysts and Its Anticancer Behavior. *Appl. Nanosci.* 2020, 10, 4221–4240. DOI: 10.1007/s13204-020-01536-2.
- [39] Jeevagan, K.; Jagannathan, K. Synthesis and Dielectric Analyses of NiS Reinforced Polyaniline Nanocomposites. *J. Mater. Sci. Mater. Electron.* 2021, 32, 27409–27421. DOI: 10.1007/s10854-021-07116-6.
- [40] Liu, W. L.; Zhang, Y. F. Blueshift of Absorption Edge and Photoluminescence in Al Doped ZnO Thin Films. *Integr. Ferroelectr.* 2018, 188(1), 112–120. DOI: 10.1080/10584587.2018.1454222.
- [41] Jiang, T.; Wang, Y.; Meng, D.; Wang, D. One-step Hydrothermal Synthesis and Enhanced Photocatalytic Performance of Pine-needle-like Zn-doped CuO Nanostructures. *J. Mater. Sci. Mater. Electron.* 2016, 27, 12884–12890. DOI: 10.1007/s10854-016-5424-2.
- [42] Andrade Neto, N. F.; Zanatta, P.; Nascimento, L. E.; Nascimento, R. M.; Bomio, M. R. D.; Motta, F. V. Characterization and Photoluminescent, Photocatalytic and Antimicrobial Properties of Boron-Doped TiO₂ Nanoparticles Obtained by Microwave-Assisted Solvothermal Method. *J. Electron. Mater.* 2019, 48, 3145–3156. DOI: 10.1007/s11664-019-07076-y.
- [43] Sharma, S.; Khare, N. Sensitization of Narrow Band Gap Bi₂S₃ Hierarchical Nanostructures with Polyaniline for Its Enhanced visible-light Photocatalytic Performance. *Colloid Polym. Sci.* 2018, 296, 1479–1489. DOI: 10.1007/s00396-018-4362-3.
- [44] Kumar, P. S.; Selvakumar, M.; Babu, S. G.; Induja, S.; Karuthapandian, S. CuO/ZnO Nanorods: An Affordable Efficient p-n Heterojunction and Morphology Dependent Photocatalytic Activity against Organic Contaminants. *J. Alloy. Compd.* 2017, 701, 562–573. DOI: 10.1016/j.jallcom.2017.01.126.
- [45] You, J. C.; Zhan, S. B.; Wen, J.; Ma, Y. W.; Zhu, Z. S. Construction of Heterojunction of Ag₂S Modified Yttrium Manganate Visible Photocatalyst and Study on Photocatalytic Mechanism. *Optik.* 2020, 217, 164900. DOI: 10.1016/j.ijleo.2020.164900.
- [46] Kinoshita, M.; Shimoyama, Y. Photocatalytic Activity of Mixed-phase Titanium Oxide Synthesized by Supercritical Sol-Gel Reaction. *J. Supercrit. Fluids.* 2018, 138, 29–35. DOI: 10.1016/j.supflu.2018.03.023.